ISSN 0021-3640, JETP Letters, 2013, Vol. 98, No. 7, pp. 403–409. © Pleiades Publishing, Inc., 2013.
Original Russian Text © V.V. Val'kov, S.V. Aksenov, E.A. Ulanov, 2013, published in Pis'ma v Zhurnal Eksperimental'noi i Teoreticheskoi Fiziki, 2013, Vol. 98, No. 7, pp. 459–465.

Effects of Multiple Reflection in the Process of Inelastic Electron Transport through an Anisotropic Magnetic Atom

V. V. Val'kov[a], *, S. V. Aksenov[a], **, and E. A. Ulanov[b]

[a] *Kirensky Institute of Physics, Siberian Branch, Russian Academy of Sciences, Akademgorodok, Krasnoyarsk, 660036 Russia*

**e-mail: vvv@iph.krasn.ru*

***e-mail: asv86@iph.krasn.ru*

[b] *Siberian State Aerospace University, pr. imeni gazety Krasnoyarskii Rabochii 31, Krasnoyarsk, 660014 Russia*

Received July 9, 2013; in final form, August 26, 2013

The effect of multiple reflection in the process of electron transport on the current–voltage characteristics of an adsorbed magnetic atom with single-ion anisotropy has been investigated. All orders of the perturbation theory with respect to the parameter of coupling between the contacts and the multilevel impurity have been taken into account by the Keldysh diagram technique with the use of Hubbard operators. It has been shown that the current–voltage characteristics of the system in a strongly nonequilibrium regime contains regions of negative differential conductance. The ways of enhancing this effect are discussed.

DOI: 10.1134/S0021364013200162

1. In studies of nanometer hybrid systems, special emphasis is put on film structures (e.g., Josephson junctions [1–3], semiconductor [4] or magnetic [5] heterojunctions) and on one- and zero-dimensional objects [6]. The current–voltage characteristics of the latter systems exhibit specific features directly related to many-body effects, which are manifested by the electron transport (Coulomb blockade, Kondo correlations [7, 8]), or to the electron–phonon interaction [9, 10]. In addition, an atomic or molecular complex with an uncompensated magnetic moment can be used for information recording and storage [11] or as a qubit [12].

The experiments on scanning tunneling microscopy of magnetic atomic and molecular complexes revealed an inelastic character of the electron transport through such systems [13]. It turned out that spin-flip scattering of transported electrons by the potential profile of the structure provides the control of its magnetic state [14]. In particular, the spin projection of the electron transported through the magnetic device (e.g., spin dimer [15]) is changed and the device occurs in another magnetic state (the dimer switches from the singlet to triplet state) owing to the spin-flip processes. In this case, the electron can be reflected back to the metallic contact and then scatter again by the already changed structure of the potential profile.

In the presence of an ensemble of electrons, one also has to take into account many-body effects when scattering of a particular electron becomes dependent on the result of interaction with the structure of other electrons. As a result of multiple recurrence of such processes, there appears an essentially nonequilibrium population distribution of the states of the magnetic system. Accordingly, there appear renormalizations of the current–voltage characteristics, which depend on the properties of the tunneling current-induced nonequilibrium state of the magnetic device. In addition, the solid-state environment, which considerably affects transport through the atomic-scale magnetic systems [11, 16], is also important.

In this work, the problem of the current–voltage characteristics of an adsorbed atom, which exhibits anisotropy of magnetic properties owing to the effect of a substrate, is solved taking into account the above factors. A large number of non-equidistant states of the system "magnetic atom + electrons" are described exactly with the use of Hubbard operators [17, 18, 7]. Nonequilibrium occupation numbers of the states of such a magnetic device are found from the set of kinetic equations derived on the basis of the Keldysh diagram technique [19] for nonequilibrium Fermi Green's functions and the diagram technique for the Hubbard operators [17, 18] modified by introducing the Keldysh loop for the nonequilibrium case [20, 21]. This approach allowed us to take into account the processes of multiple electron scattering and to derive the expression for the current which satisfies the symmetry requirements [10]. It is shown that the environment determining the crystal field can favor the enhancement of the effect of negative differential conductance. The influence of asymmetric coupling of

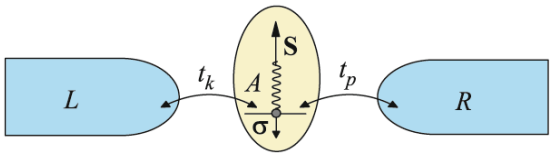

Fig. 1. Magnetic impurity with the spin S and up to two electrons on the outer shell situated between the metallic contacts.

the magnetic atom to the contacts on conducting properties of the atom is investigated.

2. We consider the tunneling transport of electrons through a magnetic impurity with the spin $S = 1$ in the geometry (see Fig. 1) used in the experiment [16, 22]. The role of such an impurity can be played by a transition-metal or rear-earth atom (e.g., Co, Mn, Fe, Ce) or a molecule in which the magnetic nucleus is surrounded by ligands (e.g., cobalt or iron phthalocyanine; Mn_{12}).

Let us write the Hamiltonian of the system "left contact + device + right contact" in the form

$$\hat{H} = \hat{H}_{\rm L} + \hat{H}_{\rm D} + \hat{H}_{\rm R} + \hat{T}, \qquad (1)$$

where the operators $\hat{H}_{\rm L}$ and $\hat{H}_{\rm R}$ include the presence of electrons in the left and right metallic contacts, respectively. In the second-quantization representation, these operators are given by the expressions

$$\hat{H}_{\rm L(R)} = \sum_{k(p)\sigma} \xi_{k(p)} c^{+}_{k(p)\sigma} c_{k(p)\sigma},$$

where $c^{+}_{k(p)\sigma}$ is the creation operator of an electron with the wave vector $k(p)$ and the spin σ in the left (right) contact and $\xi_k = \varepsilon_k - \mu$ and $\xi_p = \varepsilon_p + eV - \mu$ are the single-electron energies of the left and right contacts measured from the Fermi level μ, respectively. Below, we will assume that the contacts are single-band paramagnetic metals with the band width $W \sim 1$ eV, much greater than the characteristic energy parameters of the system. The voltage V is thought to be applied across the contacts.

The second term in Eq. (1) corresponds to the Hamiltonian of the magnetic atom ($\xi_d = \varepsilon_d + eV/2 - \mu$):

$$\hat{H}_{\rm D} = \sum_{\sigma} \xi_d n_\sigma + U n_\uparrow n_\downarrow + D(S^z)^2 + A(\boldsymbol{\sigma}\mathbf{S}), \qquad (2)$$

which describes a change in the energy of the system upon the appearance of additional electrons ($n_\sigma = a^{+}_{\sigma} a_\sigma$) in the atom, the Hubbard repulsion of two electrons with opposite spins, the effect of uniaxial anisotropy with the parameter D for the description of the experimentally established anisotropy of the magnetic properties of the impurity atom [16], and the presence of the s–$d(f)$ exchange coupling between the localized spin S of the impurity atom and the spin σ of the transported electron (the coupling strength is given by the parameter A). This coupling not only creates the additional potential profile for the transported electrons, on which they scatter, but also induces a number of phenomena leading, e.g., to the spin-dependent Fano effect [15].

The last term in Eq. (1) describes the transitions of electrons between the contacts and the magnetic impurity:

$$\hat{T} = \sum_{k(p)\sigma} t_{k(p)} [c^{+}_{k(p)\sigma} a_\sigma + \text{H.c.}], \qquad (3)$$

where t_k and t_p are the parameters of impurity coupling to the contacts and H.c. stands for the Hermitian conjugate.

3. Solving the Schrödinger equation with Hamiltonian (2), we find 12 eigenstates of an isolated magnetic impurity and electrons. Three of them are the electron-free states $\psi_1 = |0, 0\rangle$, $\psi_{2,3} = |0, \pm 1\rangle$, where the first and second numbers are the number of electrons and the projection of the total spin $\sigma + S$ of the system, respectively. The single-fermion sector of the Hilbert space contains three doubly degenerate states $\psi_{4,5} = |1, \pm 1/2\rangle_-$, $\psi_{6,7} = |1, \pm 1/2\rangle_+$, and $\psi_{8,9} = |1, \pm 3/2\rangle$. In addition, there are three two-electron states $\psi_{10} = |2, 0\rangle$ and $\psi_{11,12} = |2, \pm 1\rangle$. There are ten allowed transitions with a change in the number of electrons with the spin σ at the level of the magnetic impurity by one. Since σ does not have a preferential direction, the transition energies with opposite σ values coincide. As a result, the transition energies with $\sigma = 1/2$ are

$$\begin{aligned}
&E_{4,1} = \varepsilon_d - \nu - \Delta, \quad E_{6,1} = \varepsilon_d + \nu - \Delta,\\
&E_{5,3} = \varepsilon_d - \nu - \Delta - D, \quad E_{7,3} = \varepsilon_d + \nu - \Delta - D,\\
&E_{8,2} = \varepsilon_d + A/2, \quad E_{10,5} = \varepsilon_d + U + \nu + \Delta, \qquad (4)\\
&E_{11,4} = \varepsilon_d + D + U + \nu + \Delta, \quad E_{10,7} = \varepsilon_d + U + \Delta - \nu,\\
&E_{11,6} = \varepsilon_d + D + U + \Delta - \nu, \quad E_{12,9} = \varepsilon_d + U - A/2,
\end{aligned}$$

where $\Delta = A/4 - D/2$ and $\nu = \sqrt{\Delta^2 + A^2/2}$.

Since Hamiltonian (2) of the device includes a number of interactions, it is not diagonal in the initial representation. If this form of the Hamiltonian is used, one has to build the perturbation series not only in powers of the parameters of coupling to the contacts but also in the parameters characterizing the internal interactions in the device. However, reduction of the Hamiltonian of the device to the diagonal form in the usual representation leads to the situation where the Fermi operator of electron annihilation in the device in the interaction representation is described by the expression that prevents the direct implementation of the Vick theorem. Overcoming this hindrance is associated with the use of the atomic representation. In the

mathematical language, this corresponds to introducing the Hubbard operators X^{α}, where $\alpha = \alpha(n, m)$ and n and m specify the initial and finite states of the transition $\alpha(n, m)$ [18]. In this case, the second-quantization operators a_{σ} of electron annihilation at the impurity are described in terms of the Hubbard operators with the use of the respective representation parameters $\gamma_{\sigma}(\alpha)$. Thus, the Hamiltonian of the structure in the atomic representation has the simple form $\hat{H}_{\mathrm{D}} = \sum_{l} E_l X^{ll}$.

4. We use the well-known definition of the electric current $I = edN_{\mathrm{L}}/dt$. After simple transformations and the implementation of the atomic representation, we come to the expression that is convenient for practical calculations:

$$I = ie\sum_{k\sigma,\,\alpha} t_k\gamma_{\sigma}(\alpha)\left[e^{i\frac{eV}{2}t}\langle X^{-\alpha}c_{k\sigma}\rangle - e^{-i\frac{eV}{2}t}\langle c^{+}_{k\sigma}X^{\alpha}\rangle\right]. \quad (5)$$

Equation (5) takes into account that, under the passage of the electric current, when the electron is transported from a contact to the device, the latter changes its state and switches to the other sector of the Hilbert space with the number of electrons increased by one. Many transitions of this kind can exist. All of them generally give a nonzero contribution. This is taken into account by including the sum over the variable α into Eq. (5). Hereinafter, $\hbar = 1$.

The averages involved in Eq. (5) can be expressed in terms of nonequilibrium mixed Green's functions $G^{+-}_{k\sigma,\,\alpha}(t_+,\ t_-) = -i\langle \hat{T}_C c_{k\sigma}(t_+)X^{-\alpha}(t_-)S_C\rangle_0$ and $G^{+-}_{\alpha,\,k\sigma}(t_+,\ t_-) = -i\langle \hat{T}_C X^{\alpha}(t_+)c^{+}_{k\sigma}(t_-)S_C\rangle_0$, where $S_C = \hat{T}_C\exp[-i\int_C d\tau\,\hat{T}(\tau)]$ [19]. The times t_+ and t_- $(t_+ < t_-)$ are situated at the lower branch of the Keldysh loop C. It can be shown by analyzing the diagrammatic series for the mixed Green's functions $G^{+-}_{k\sigma,\,\alpha}$ and $G^{+-}_{\alpha,\,k\sigma}$ that these functions are proportional to the product of the Green's function $G_{k\sigma}(\tau - \tau') = -i\langle \hat{T}_C c_{k\sigma}(\tau)c^{+}_{k\sigma}(\tau')\rangle_0$ of the left contact and the Green's function $D_{\alpha\beta}(\tau - \tau') = -i\langle \hat{T}_C X^{\alpha}(\tau)X^{-\beta}(\tau')\rangle_0$ of the structure. Thus, the expression for the current after the Fourier transformation reads

$$I = e\sum_{k\sigma,\,\alpha\beta} t_k^2\gamma_{\sigma}(\alpha)\gamma_{\sigma}(\beta)\int_{-\infty}^{+\infty}\frac{d\omega}{2\pi}$$
$$\times\left[G^{-+}_{k\sigma}(\omega)D^{+-}_{\alpha\beta}\left(\omega - \frac{eV}{2}\right)\right. \quad (6)$$
$$\left. - G^{+-}_{k\sigma}(\omega)D^{-+}_{\alpha\beta}\left(\omega - \frac{eV}{2}\right)\right].$$

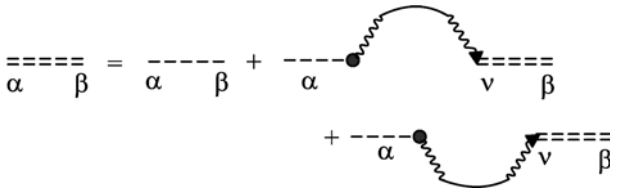

Fig. 2. Dyson equation for the Green's function $D_{\alpha\beta}(\omega)$.

It is noteworthy that the third- and higher order perturbations should be taken into account in order to obtain an expression for the current naturally symmetrized with respect to t_k and t_p. This was mentioned, in particular, in [10]. The multiple scattering processes were included in all orders of perturbation theory with respect to t_k and t_p by solving the Dyson equation for the Green's function $D_{\alpha\beta}(\omega)$. This equation is shown in the diagrammatic form in Fig. 2. The double dashed line corresponds to the full Green's function $D_{\alpha\beta}(\omega)$, the dashed line represents the bare function $D_{0\alpha}(\omega)$, the solid line bended upward (downward) is the Green's function $G_{k(p)\sigma}(\omega \pm eV/2)$ of the isolated left (right) contact, and the wavy line is the factor $t_{k(p)}\gamma_{\sigma}(\alpha)$. Taking into account the summation over the variables referred to all internal vertices, we find the following expressions for the components of the mass operator:

$$\Sigma^{++}_{\alpha\nu} = \Sigma^{--}_{\alpha\nu} = i\sum_{j\,=\,L,\,R;\,\sigma}\gamma_{\sigma}(\alpha)\gamma_{\sigma}(\nu)(2n_j - 1)\Gamma^{j},$$

$$\Sigma^{+-}_{\alpha\nu} = -2i\sum_{j\,=\,L,\,R;\,\sigma}\gamma_{\sigma}(\alpha)\gamma_{\sigma}(\nu)n_j\Gamma^{j}, \quad (7)$$

$$\Sigma^{-+}_{\alpha\nu} = 2i\sum_{j\,=\,L,\,R;\,\sigma}\gamma_{\sigma}(\alpha)\gamma_{\sigma}(\nu)(1 - n_j)\Gamma^{j},$$

where $\Gamma^{j}(\omega) = 4t_j^2 g_j\sqrt{1 - 4(\omega + \mu)^2/W^2}$ is the parameter of the level broadening of the system owing to the coupling to the jth contact, n_j is the Fermi–Dirac distribution function of the jth contact, g_j is the density of states of the jth contact, and t_j is the parameter of electron hopping from the last node of the jth contact to the level of the magnetic atom. In Eq. (7), we used the approximation of wideband contacts. This implies that we neglected the level shift in the analysis of the effect of the contacts on the levels of our structure. In addition, this allows us to neglect the frequency dependence of the level broadening in particular calculations. In this case, as is often assumed, $\Gamma^{j} \simeq \pi t_j^2 g_j$.

Acting by the operator $\hat{D}^{-1}_{0\alpha} = i\frac{\partial}{\partial t} + E_{\alpha}$ on the Dyson equation (by the analogy with [19]) and solving

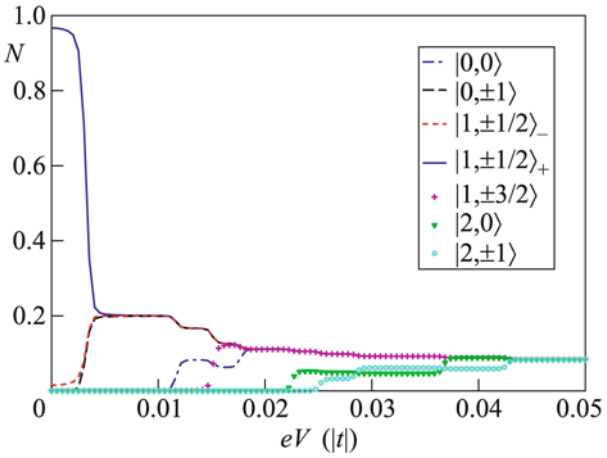

Fig. 3. Nonequilibrium occupation numbers for the states of the system "magnetic impurity + electrons" with the parameters $t = -1$ eV, $t_L = t_R = t/100$, $\varepsilon_d = A = 0.005\ |t|$, $D = 0.003\ |t|$, $U = 0.01\ |t|$, and $T = 1$ K.

the resulting set of equations with respect to $D^{+-}_{\alpha\beta}(\omega - eV/2)$ and $D^{-+}_{\alpha\beta}(\omega - eV/2)$, we find the expression describing the electron current through the magnetic atom

$$I = 2e\sum_{\sigma,\alpha\beta}\int_{-\infty}^{+\infty}\frac{d\omega}{\pi}\frac{\Gamma^L\Gamma^R L_{\sigma,\alpha}L_{\sigma,\beta}}{1+\left[\sum_\nu \Gamma L_{\sigma,\nu}\right]^2}$$

$$\times [n_R(\omega - eV) - n_L(\omega)],$$

$$L_{\sigma,\alpha} = \frac{b_\alpha\gamma^2_\sigma(\alpha)}{\omega - eV/2 + E_\alpha}, \qquad (8)$$

$$b_\alpha = N_n + N_m, \quad \Gamma = \Gamma^L + \Gamma^R.$$

Here, $E_\alpha = E_n - E_m$ if α corresponds to the transition of the magnetic atom from the state m to the state n; i.e., $\alpha = \alpha(n, m)$. It is noteworthy that Eq. (8) is symmetric with respect to t_L and t_R.

The appearance of the renormalized end factor shown by the dark circle in Fig. 2 is associated with nonequilibrium processes leading to multiple scattering. Therefore, the occupation numbers N_n and N_m of the nth and mth states of the system turn out to depend not only on the temperature T and the parameters of the system but also on the remaining occupation numbers. To find $N_1, N_2, \ldots, N_{12}$, the following set of kinetic equations is solved under the additional condition $\sum_{i=1}^{12} N_i = 1$:

$$N_m = \frac{1}{2\pi i}\int_{-\infty}^{+\infty} d\omega D^{+-}_{\alpha\alpha}(\omega)$$

$$\simeq \sum_\sigma \int_{-\infty}^{+\infty}\frac{d\omega}{\pi\Gamma}\frac{b_\alpha\kappa_{\sigma,\alpha}[\Gamma^L n_L(\omega) + \Gamma^R n_R(\omega - eV)]}{(\omega + \omega_{\sigma,\alpha})^2 + \kappa^2_{\sigma,\alpha}}. \qquad (9)$$

Here,

$$\omega_{\sigma,\alpha} = E_\alpha - eV/2 + \lambda_{\sigma,\alpha}\kappa_{\sigma,\alpha},$$

$$\kappa_{\sigma,\alpha} = \frac{\Gamma\gamma^2_\sigma(\alpha)b_\alpha}{1+\lambda^2_{\sigma,\alpha}}, \quad \lambda_{\sigma,\alpha} = \sum_{\beta\neq\alpha}\frac{b_\beta\gamma^2_\sigma(\beta)\Gamma}{E_\beta - E_\alpha}.$$

In the region $T \ll E_\alpha$, the integral in Eq. (9) can be evaluated analytically and the set of kinetic equations is represented in the simpler form

$$N_m = \sum_\sigma \frac{b_\alpha}{\pi}\left[\arctan\left(\frac{W/2 - eV/2 - \omega_{\sigma,\alpha}}{\kappa_{\sigma,\alpha}}\right)\right.$$

$$\left. + \frac{\Gamma^L}{\Gamma}\arctan\left(\frac{\omega_{\sigma,\alpha}}{\kappa_{\sigma,\alpha}}\right) + \frac{\Gamma^R}{\Gamma}\arctan\left(\frac{\omega_{\sigma,\alpha} + eV}{\kappa_{\sigma,\alpha}}\right)\right]. \qquad (10)$$

Below, we perform the numerical calculations of the transport characteristics of the magnetic impurity in the weak-coupling regime $\Gamma^L, \Gamma^R \ll E_\alpha$, which is most important for applications. In this case, broadening of the energy levels of the system is much smaller than the energy difference between these levels. As is seen from the definition of the quantities $\Gamma^L = \pi g_L t_L^2$, $\Gamma^R = \pi g_R t_R^2$, the smallness of the products $g_R t_R$, $g_L t_L \ll 1$ allows one to separate two cases. In the first case, the weak-coupling regime takes place even if $A < t_L, t_R$. In the second case, $A > t_L, t_R$ and the possibility of weak coupling is obvious.

The reality of the first case follows from comparison of the results of theoretical and experimental works. According to the theoretical estimates [23, 24], $A \sim 10^{-4}$–10^{-3} eV. On the other hand, as follows from the experimental works [25, 26], in the weak-coupling regime, $\Gamma^L, \Gamma^R \sim 10^{-5}$–$10^{-4}$ eV. Then, taking $g_{L(R)} \simeq 1/W$, we find $t_L, t_R \sim 10^{-2}$ eV and $A < t_L, t_R$.

The dependence of the occupation numbers N_1, N_2, ... on the energy eV of the bias electric field in the first case is shown in Fig. 3. The energy parameters of the impurity were chosen such that at $D > 0$ the impurity does not contain electrons in the zeroth approximation with respect to t_L, t_R, the ground state is the singlet $|0, 0\rangle$, and $N_1 = 1$. With the inclusion of multiple reflection, N_1 decreases even at $V = 0$ (solid line in Fig. 3). An increase in the bias field leads to a shift of the energy levels of the impurity. At each value of the electric field satisfying the condition $eV/2 \sim E_\alpha$, the transition of the impurity system from the state with the number r to the state with the number l (presum-

ably, $\alpha = \alpha(l, r)$) becomes possible. As a result, the occupation number N_l increases and the other occupation numbers decrease. This leads to the stepwise behavior of the occupation numbers shown in Fig. 3. In addition, the populations of all previously excited states undergo sharp changes in the vicinity of the "resonance" values of the electric field. Thus, at high voltages, the impurity subsystem can occur with equal probability in each of the 12 states.

Considered features produce the stepwise current–voltage characteristics similar to that observed in the case of Coulomb blockade. The results of the calculation of the current–voltage characteristics for two signs of the anisotropy parameter D are shown in Fig. 4. These curves agree with the experimental data obtained by studying the transport through individual molecular magnets [22]. Each step indicates opening of an additional channel for the transmission of the electron and occurs at the above-mentioned resonance values of the bias field, when $eV/2 \sim E_\alpha$.

An essential feature of the calculated current–voltage characteristics is that, as in the experiment [22], there are the regions of negative differential conductance. For a better visibility, the presence of negative differential conductance is shown in the inset in Fig. 4.

Let us discuss the origin of negative differential conductance. As follows from Eq. (8), the current is the sum of the diagonal ($I_{\alpha\alpha}$) and off-diagonal ($I_{\alpha\beta}$) partial components. According to numerical estimates, $I_{\alpha\alpha} \gg I_{\alpha\beta}$. The partial contribution $I_{\alpha\alpha}$ to the current associated with the channel corresponding to the transition of the impurity system from the state r to the state l (i.e., to the root vector $\alpha(l, r)$) can be written in the form

$$I_{\alpha\alpha} \simeq \frac{2e}{\pi}\frac{\Gamma^L\Gamma^R}{\Gamma}\sum_\sigma b_\alpha\gamma_\sigma^2(\alpha)\left[\arctan\left(\frac{E_\alpha + eV/2}{\Gamma b_\alpha\gamma_\sigma^2(\alpha)}\right)\right. \\ \left. - \arctan\left(\frac{E_\alpha - eV/2}{\Gamma b_\alpha\gamma_\sigma^2(\alpha)}\right)\right]. \quad (11)$$

This implies that, at the bias field below the resonance value ($eV/2 < E_\alpha$), $I_{\alpha\alpha} = 0$.

Over the transition through the resonance bias field ($eV/2 > E_\alpha$), the argument of the second arctangent changes its sign and

$$I_{\alpha\alpha} \sim \frac{\Gamma^L\Gamma^R}{\Gamma}\sum_\sigma b_\alpha\gamma_\sigma^2(\alpha). \quad (12)$$

Obviously, a change in the partial current in the open channel is associated with a change in the end factor defined as the sum of the occupation numbers. Since the number of nonzero occupation numbers increases under the transition through the resonance value of the bias field, the occupation numbers that were nonzero before the transition decrease owing to the above-mentioned completeness condition. This implies a decrease in the partial currents $I_{\beta\beta}$ for the channels that were open before the particular transition. In view of these circumstances, the condition of the appearance of negative differential conductance can be easily written as

$$\sum_\beta I_{\beta\beta}(V_1) > \sum_\beta I_{\beta\beta}(V_2) + I_{\alpha\alpha}(V_2), \quad V_1 < V_2. \quad (13)$$

It is noteworthy that the effect of negative differential conductance depends on the sign of the anisotropy constant D. Consequently, considerable modification of the transport properties of a magnetic atom or a molecule can be achieved by changing their crystal environment, e.g., by placing them in topologically nonequivalent sites on a substrate [16].

In the second case ($t_L, t_R < A$), the fulfillment of the weak-coupling condition is obvious. The behavior of the current–voltage characteristics remains qualitatively similar to that considered above. Importantly, the regions of negative differential conductance also persist in this regime (see Fig. 5).

If $t_L \neq t_R$, a considerable amplification of the effect of negative differential conductance takes place in addition to the asymmetry of the current–voltage characteristics (see the region of $eV \sim -0.02|t|$ in Fig. 6). In this case, the voltage dependence of the occupation numbers is also asymmetric with respect to a change in polarity. At $V > 0$, the electrons move toward the left contact. However, their tunneling from the right contact to the impurity orbital is suppressed because $t_R \ll t_L$. This leads to the absence of electrons in the central region, i.e., to the preferential occupation of the states $|0, 0\rangle$ and $|0, \pm1\rangle$ at high V values. This situation for $D > 0$ is illustrated in Fig. 7. In the

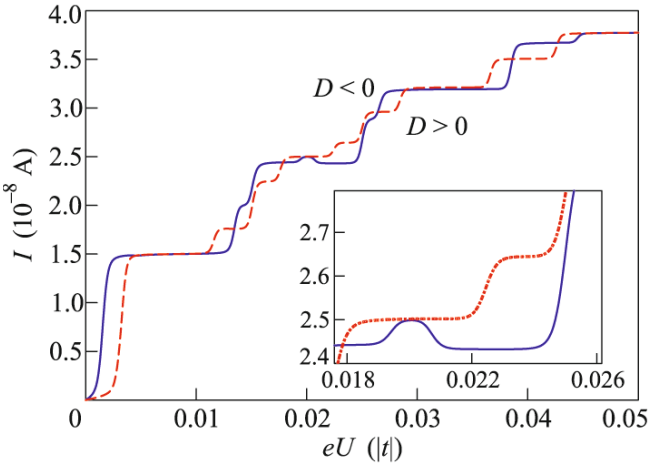

Fig. 4. Current–voltage characteristics of the magnetic impurity at D = (dashed line) 0.003 $|t|$ and (solid line) $-0.003\ |t|$; the other parameters are the same as in Fig. 3. The inset shows the region of negative differential conductance at $D < 0$.

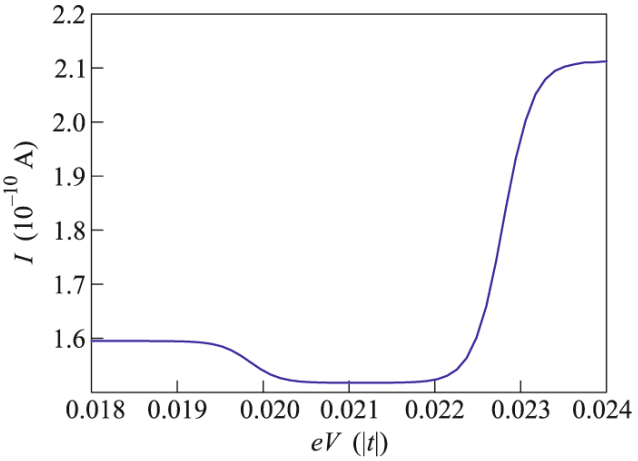

Fig. 5. Region of the current–voltage characteristics of the magnetic impurity with negative differential conductance for the case of t_L, $t_R < A$ at the parameters $t = -1$ eV, $t_L = t_R = t/1000$, $\varepsilon_d = 0.008\,|t|$, $A = 0.011\,|t|$, $D = -0.009\,|t|$, $U = 0.01\,|t|$, and $T = 1$ K.

opposite case (under change of the sign of V), the states with two electrons become dominant.

It is noteworthy that the possibility of consecutive switching between various states of the system under the action of the electric field is essential for information recording and storage. An almost 100% transition from the ground electron-free state $|0, 0\rangle$ to the magnetic single-electron state $|1, \pm 1/2\rangle_-$ (the behavior of the population of this state is shown by the dashed line in Fig. 7) without the preferential direction of the total spin occurs under a decrease in V below zero. Under a further decrease in the region $eV \sim -0.025|t|$, the system with a high probability can be in the nonmagnetic two-electron state $|2, 0\rangle$ (the respective curve is shown by triangles).

5. In conclusion, we discuss a number of specific features of the above calculations. The main feature is associated with the fact that, owing to the s–f exchange coupling between the spins of the transported electron and impurity, the passage of the tunneling current through the magnetically active atom is accompanied by inelastic processes leading to the excitation of upper energy states of the impurity center. Therefore, the tunneling characteristics of the system under investigation in the steady state are determined by both scattering on the ground state of the impurity center and the processes involving the excited states. In this case, multiple scattering processes, in which the electron after reflection and transfer of the impurity center to the excited state experiences secondary scattering by the transformed structure of the magnetic ion owing to a change in the occupation probability of the states, become significant.

In this work, inelastic processes and the effects of multiple reflection are described on the basis of the combination of the Keldysh method for the calculation of nonequilibrium Green's functions and the ideology of atomic representation with the use of diagram technique for Hubbard operators [17, 18]. The inclusion of the atomic representation turned out to be quite effective for the description of inelastic processes under the quantum transport through the magnetic atom, since it allows one to represent the multilevel Hamiltonian of the impurity center in the diagonal form. In addition, the terms corresponding to the contributions of all scattering channels are involved in the theory explicitly. As a result, it proves possible to derive the closed system of transcendental quantum kinetic

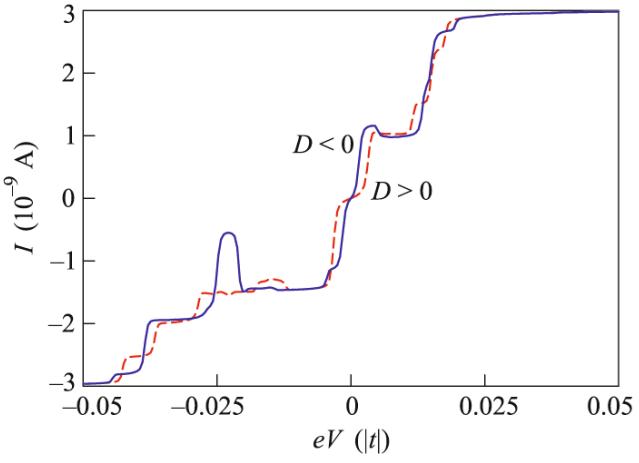

Fig. 6. Current–voltage characteristics of the magnetic impurity for the case of asymmetric coupling with the contacts: $t_L = t/50$, $t_R = t_L/10$; the other parameters are the same as in Fig. 4.

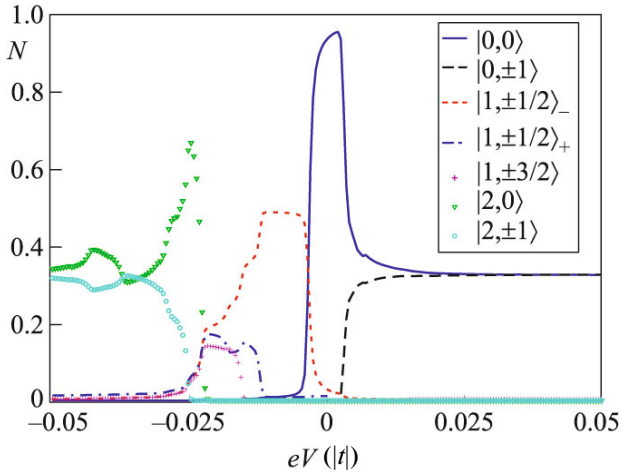

Fig. 7. Nonequilibrium occupation numbers of the states of the system at $D > 0$; the other parameters are the same as in Fig. 6.

equations which determine implicitly the nonequilibrium occupation numbers of the structure.

The calculation of the current–voltage characteristics in the weak-coupling regime has shown that the possibility of the occupation of the excited states of the system "magnetic atom + electrons" by intensification of nonequilibrium inelastic scattering leads to the stepwise behavior of the current–voltage characteristics and induces negative differential conductance. The effects found in this work agree with those observed in experiments on the transport through individual molecular magnets [22].

It has been mentioned that the magnitude of the effect of negative differential conductance depends strongly on both the solid-state environment of the magnetic ion and the parameters of coupling to the metallic contacts. Based on this fact, it has been predicted that the atomic-size magnetic object with an asymmetric coupling to the contacts can be used to record information.

This work was supported by the Presidium of the Russian Academy of Sciences (program "Quantum Mesoscopic and Disordered Systems"), the Ministry of Education and Science of Russian Federation (state contract no. 16.740.11.0644, federal program "Human Capital for Science and Education in Innovative Russia" for 2009–2013), and the Russian Foundation for Basic Research (project nos. 12-02-31130, 13-02-00523, and 13-02-98013). S.V.A. is grateful to the Council of the President of the Russian Federation for Support of Young Scientists and Leading Scientific Schools, project nos. MK-526.2013.2 and SP-6361.2013.5.

REFERENCES

1. Y. Makhlin, G. Schon, and A. Shnirman, Rev. Mod. Phys. **73**, 357 (2001).
2. V. F. Gantmakher and V. T. Dolgopolov, Phys. Usp. **53**, 1 (2010).
3. A. K. Feofanov, V. A. Oboznov, V. V. Bol'ginov, et al., Nature Phys. **6**, 593 (2010).
4. I. V. Rozhansky, N. S. Averkiev, and E. Lahderanta, Low Temp. Phys. **39**, 40 (2013).
5. S. N. Vdovichev, B. A. Gribkov, S. A. Gusev, et al., JETP Lett. **94**, 386 (2011).
6. J. Park, A. N. Pasupathy, J. I. Goldsmith, et al., Nature **417**, 722 (2002).
7. K. Kikoin and Y. Avishai, Phys. Rev. Lett. **86**, 2090 (2001).
8. P. I. Arseyev, N. S. Maslova, and V. N. Mantsevich, JETP Lett. **94**, 390 (2011).
9. H. Ueba, T. Mii, and S. G. Tikhodeev, Surf. Sci. **601**, 5220 (2007).
10. P. I. Arseev and N. S. Maslova, Phys. Usp. **53**, 1151 (2010).
11. S. Loth, S. Baumann, C. P. Lutz, et al., Science **335**, 196 (2012).
12. J. Tejada, E. M. Chudnovsky, E. del Barco, and J. M. Hernandez, Nanotechnology **12**, 181 (2001).
13. A. J. Heinrich, J. A. Gupta, and C. P. Lutz, Science **306**, 466 (2004).
14. S. Loth, K. von Bergmann, M. Ternes, et al., Nature Phys. **6**, 340 (2010).
15. V. V. Val'kov and S. V. Aksenov, J. Exp. Theor. Phys. **113**, 266 (2011); V. V. Val'kov, S. V. Aksenov, and E. A. Ulanov, J. Exp. Theor. Phys. **116**, 954 (2013).
16. A. F. Otte, M. Ternes, K. von Bergmann, et al., Nature Phys. **4**, 847 (2008).
17. R. O. Zaitsev, Sov. Phys. JETP **41**, 100 (1975).
18. R. O. Zaitsev, Sov. Phys. JETP **43**, 574 (1976).
19. L. V. Keldysh, Sov. Phys. JETP **20**, 1018 (1964).
20. R. O. Zaitsev, *Introduction to Modern Kinetic Theory, Course of Lectures* (KomKniga, Moscow, 2007) [in Russian].
21. J. Fransson, O. Eriksson, and I. Sandalov, Phys. Rev. Lett. **88**, 226601 (2002).
22. H. B. Heersche, Z. de Groot, J. A. Folk, et al., Phys. Rev. Lett. **96**, 206801 (2006).
23. K. Park and M. R. Pederson, Phys. Rev. B **70**, 054414 (2004).
24. F. Qu and P. Hawrylak, Phys. Rev. Lett. **95**, 217206 (2005).
25. J. Gores, D. Coldhaber-Gordon, S. Heemeyer, and M. A. Kastner, Phys. Rev. B **62**, 2188 (2000).
26. I. G. Zacharia, D. Goldhaber-Gordon, G. Granger, et al., Phys. Rev. B **64**, 155311 (2001).

Translated by A. Safonov